

Research article

# Nonterminal liquid crystalline epoxy resins as structurally ordered low $T_g$ thermosets with potential as smart polymers

Maciej Kisiel<sup>1\*</sup>, Weronika Zajęc<sup>2</sup>, Magdalena Włodarska<sup>3</sup>, Łukasz Byczyński<sup>1</sup>,  
Dominika Czachor-Jadacka<sup>1</sup>, Beata Mossety-Leszczak<sup>1</sup>, Gabriela Pietruszewska<sup>1</sup>,  
Magda Drożdziel-Jurkiewicz<sup>4</sup>, Jarosław Bienias<sup>4</sup>

<sup>1</sup>Rzeszów University of Technology, Faculty of Chemistry, al. Powstańców Warszawy 6, 35-959 Rzeszów, Poland

<sup>2</sup>Doctoral School of the Rzeszów University of Technology, al. Powstańców Warszawy 12, 35-959 Rzeszów, Poland

<sup>3</sup>Lodz University of Technology, Institute of Physics, Wólczajska 217/221, 93-005 Łódź, Poland

<sup>4</sup>Lublin University of Technology, Faculty of Mechanical Engineering, Nadbystrzycka 36, 20-618 Lublin, Poland

Received 15 January 2024; accepted in revised form 13 February 2024

**Abstract.** Novel nonterminal liquid crystalline epoxy resin has been synthesized, and its structure and nature have been determined via nuclear magnetic resonance (NMR) and polarized optical microscopy (POM). Then, it was cured with the use of 4,4'-diaminodiphenylmethane (4,4'-DDM). The curing process has been investigated via differential scanning calorimetry (DSC) and infrared spectroscopy (FTIR) methods. Polymerization has been conducted with (1.2 T) and without the presence of a strong magnetic field. The properties of the obtained polymers have been described using DSC, thermogravimetric analysis (TGA), scanning electron microscopy (SEM), dielectric spectroscopy (DS) and X-ray scattering studies (WAXS/SAXS). It has been proved that the magnetic field induces molecular ordering and increases the glass transition temperature ( $T_g$ ) by over 20 °C. The obtained ordered polymers are thermally stable up to over 300 °C, undergo vitrification at slightly elevated temperature (37.5 °C), and their electrical conductivity rises significantly at the transition to an elastic state, which, among other possibilities, makes them a proper candidate for a smart, lightweight polymers with tuneable properties by a subtle temperature rise and possibility of tailoring its structure by a magnetic field.

**Keywords:** epoxy, liquid crystal polymer, thermoset, crosslinking, curing, thermal analysis, molecular order

## 1. Introduction

Epoxy resins are one of the most common and useful thermosetting materials and have been studied thoroughly for many decades [1, 2]. They offer unique adhesive, thermal and mechanical properties, but more importantly, they are suitable for tailoring them to a specific need. The literature presents examples of modifications to achieve the desired thermal stability and glass transition temperature [3], flame retardancy [3–5], mechanical properties [6], etc. However, traditional epoxies lack smart properties offered by liquid crystalline epoxy resins (LCER), which are state-of-the-art materials with superior

properties in comparison with their traditional versions. They have been studied since the 1990s, and their potential seems to be unsurpassed. Over the last years, several comprehensive reviews [7, 8] and book chapters [9] have emerged that describe their various advantages and possibilities. Most of them come from the liquid-crystalline (LC) nature of those compounds. They are possible to order structurally due to mechanical tension [10] or in the presence of an external force field [11, 12], and this arrangement gives them anisotropic properties of various kinds (e.g. mechanical strength, electrical conductivity, heat conductivity, optical properties – generally enhanced

R1  
R2  
R3  
R4  
R5  
R6  
R7  
R8  
R9  
R10  
R11  
R12  
R13

\*Corresponding author, e-mail: [m.kisiel@prz.edu.pl](mailto:m.kisiel@prz.edu.pl)

© BME-PT

alongside the orientation axis) as well as makes them susceptible to UV radiation [13]. Ordered and conducting polymers are often proposed as a starting material for advanced electronic devices with examples presented in the literature, like flexible films for electronic use, supercapacitors, solar cells, OLEDs, low dielectric thermosets or substrates for 5G antennas [14–17]. The use of smart polymers, which may be reusable [18], is destined to grow in the future due to the wide range of applications from attenuators [19], shape memory [20, 21], self-healing and cleaning materials [22] and all modern electronics as mentioned before, as well as some highly specific uses, such as the production of lactose-free milk [23].

Our research team has been pursuing this topic for some time now, and we determined how efficiently molecular order can be achieved [24] and how it is possible to synthesize polymers that are characterized by interesting and valuable features (increased mechanical strength) and applications, *e.g.* substrate for powder coating [25, 26]. We were also, similarly to this paper, describing electrical properties of synthesized polymers [27] but we struggled with the relatively high glass transition temperature ( $T_g$ ) fluctuating about 80°C regardless of the composition of a sample. This paper presents a solution to this problem, an introduction of nonterminal LCER that we have found no evidence of in the literature so far. This allows the  $T_g$  to be reduced to the ambient temperature region, and the use of oleic acid in the synthesis process is in compliance with the principles of green chemistry, which is rarely the case when epoxy resins are taken into consideration. The first results were presented with a three-aromatic mesogenic resin with even lower  $T_g$  and interesting dielectric studies [28]. This paper describes a four-aromatic (the centre of the mesogen is created from a biphenyl and two molecules of *p*-hydroxybenzoic acid instead of hydroquinone and two molecules of *p*-hydroxybenzoic acid – hence one more aromatic ring) nonterminal LCER with potential as a smart polymer. The incorporation of biphenyl in place of hydroquinone is causing more stiff nature of the core of obtained polymers and visibly increases especially their glass transition temperature. The term ‘non-terminal’ means that epoxy groups are located in the middle of the aliphatic chain, which is a significant novelty and a clear enrichment of knowledge. So far, described resins have epoxy groups located at the end of aliphatic chains. This innovation has brought

a new possibility to the forefront. Now it is feasible to create a shift of the properties by more than 50°C only with the introduction of nonterminal epoxy groups with exactly the same core of the molecule. Moreover, dangling aliphatic chains are bringing more elasticity to the polymer, which is described in detail later in this manuscript. All of the acquired data is presented for the first time for this novel resin, which allows the production of tailored polymers with low crosslink density as a result of their structure and combined with its bigger elasticity.

## 2. Materials and methods

### 2.1. Materials

4,4'-dihydroxybiphenyl was supplied by Glentham Life Sciences, Corsham, Great Britain. Oleic acid was supplied by Fisher Chemical, Loughborough, Great Britain. *N,N'*-dicyclohexylcarbodiimide (DCC), *p*-hydroxybenzoic acid, *p*-toluenesulfonic acid (*p*-TSA), 4-(dimethylamino)pyridine (DMAP), *m*-chloroperbenzoic acid (MCPBA) and 4,4'-diaminodiphenylmethane (4,4'-DDM) were supplied by Sigma Aldrich, Darmstadt, Germany. Ethanol, methanol, ethyl acetate, dichloromethane and acetone were supplied by Chempur, Piekary Śląskie, Poland.

### 2.2. LCER synthesis

The synthesis was conducted in a three-step process presented in Figure 1.

In the first step, the stoichiometric amounts of 4,4'-dihydroxybiphenyl (34.11 g; 0.1832 mol) and *p*-hydroxybenzoic acid (50.60 g; 0.3664 mol) as well as 0.34 g (0.002 mol) of *p*-toluenesulfonic used as catalyst, were mixed without any solvent in a round bottom four-neck flask equipped with a nitrogen gas inlet. The mixture was vigorously stirred with a mechanical stirrer and heated until the substrates melted (more than 270°C). After melting, the process was continued for about 15 min. The crude brown product was cooled, ground in a mortar and mixed in boiling ethanol for purification. The mixture was filtered under vacuum and the product marked as MEZO III was excessively rinsed with hot ethanol until it became white. After drying, 49.50 g of white/grey product was obtained (63% yield).

In the second step, 4.26 g (0.01 mol) of MEZO III, 5.65 g (0.02 mol) of oleic acid, 4.54 g of DCC (0.022 mol – 10% excess), 0.12 g (0.00 mol) of DMAP used as a catalyst and 100 ml of dichloromethane were placed in a three neck round bottom

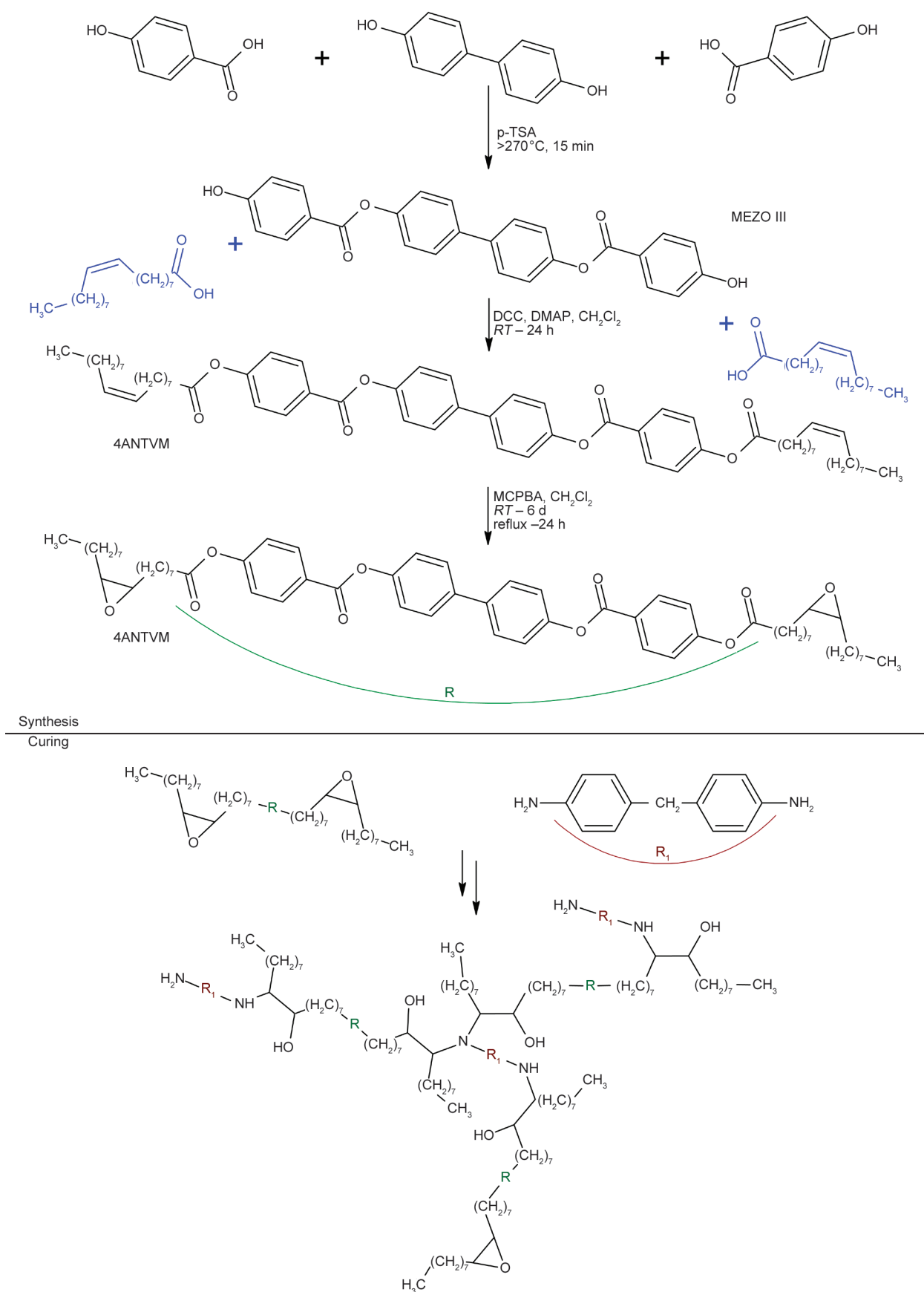


Figure 1. Synthesis route and curing reaction of a nonterminal liquid crystalline epoxy resin – 4ANTEM.

flask and stirred in ambient temperature for 24 h. The mixture was then filtered under vacuum and the solvent from the filtrate was removed with the use of a rotary evaporator. The crude product was mixed for 15 min in 100 ml of boiling methanol, filtered and dried. 6.98 g (0.007 mol) of white solid was obtained (73% yield). The product was named 4ANTVM (four-aromatic nonterminal vinyl monomer).

In the last step of the synthesis, 9.533 g (0.01 mol) of 4ARNTM, 7.17 g (0.27 mol) of MCPBA (35% excess calculated with the assumption that the substrate purity is 65% due to its decomposition with time) and 100 ml of dichloromethane were placed in a three neck round bottom flask and stirred with magnetic stirrer for six days at room temperature and then under reflux for the last 24 h. The mixture was cooled, filtered under vacuum and the filtrate was washed in a three-step manner subsequently with 80 ml of 5% sodium sulfite solution, 80 ml of 5% sodium hydrogen carbonate solution and 80 ml of saturated NaCl solution. After each washing, the organic layer was separated. Finally, the organic layer was dried with magnesium sulfate and the drying agent was filtered. The solvent was removed with the use of a rotary evaporator. The crude product was purified by mixing with 150 ml of boiling ethyl acetate, cooling and filtrating. After that, the purification procedure was repeated with 150 ml of methanol. 7.88 g (0.008 mol) of white solid named 4ANTEM (four-aromatic nonterminal epoxy monomer) was obtained (80% yield).

### 2.3. Sample preparation for curing

To prepare thermoset samples, 2 g of 4ANTEM mixture and a stoichiometric amount of 4,4'-DDM were mixed with 15 ml of acetone and stirred for 2 h. The solvent was then evaporated at room temperature and the mixture prepared was stored at approximately 10 °C before curing. 125 mg of 4ANTEM/4,4'-DDM samples were placed in Teflon molds (5×4×8.5 mm) and cured for 3 h at 205 °C. The samples were cured in a magnetic field using the RTM-1 device from REMEL S.C. Nowy Targ, Poland, equipped with neodymium magnets capable of providing a homogeneous magnetic field in small volume. During the crosslinking process, the compositions were heated in an oven, with a magnetic field of 1.2 T and 0 T applied to the oven. After cure, the samples were

allowed to cool to room temperature with the magnetic field still applied. Curing reaction is presented at the bottom of the [Figure 1](#).

## 2.4. Characterization

### 2.4.1. <sup>1</sup>H-NMR analysis

Proton nuclear magnetic resonance NMR experiments were carried out using an Avance II Plus, Bruker, Billerica, USA spectrometer operating at 500.13 MHz under a static magnetic field of 11.7 T. Spectra were obtained on a spectrometer using standard instrument software (Topspin 1.3) and pulse sequences (zg30), at a probe temperature of 25 °C. The typical acquisition parameters for proton NMR experiments were as follows: acquisition time 3.27 s, spectral width 4000–6000 Hz, nutation angle 30°, relaxation delay 1 s, 32 K data points. A 30 degree single pulse sequence was used for FID accumulation. For all samples studied in this report, a small piece (3 to 5 mg) was dissolved in 0.6 ml of CDCl<sub>3</sub> using 5 mm NMR tubes. Chemical shifts were expressed in ppm downfield from tetramethylsilane (TMS) as an internal reference. Deuterated solvent with deuterium isotope enrichments of 99.6% were purchased from ARMAR Chemicals, Jakobiho, Czech Republic.

### 2.4.2. DSC analysis

DSC analyses were performed with the DSC822<sup>e</sup>, Mettler Toledo, Greifensee, Switzerland instrument, in a nitrogen atmosphere, with a nitrogen gas flow of 60 ml/min. The heating rate was 5 °C/min with the exception related to the determination of the glass transition temperature, where the 10 °C/min rate was used. The temperature range of the measurements was individually selected for each experiment and are presented on every thermogram. The weight of the samples was about 10–20 mg.

### 2.4.3. FT-IR analysis

FT-IR measurements were taken with use of a Nicolet 6700 FT-IR, Thermo Scientific, Waltham, USA spectrophotometer by the attenuated total reflection method. Spectra were recorded within the 400–4000 cm<sup>-1</sup> wavenumber range. Spectra were evaluated using F. Menges 'Spectragryph – optical spectroscopy software', Version 1.2.16.1, 2023, <http://www.effemm2.de/spectragryph/>.

#### 2.4.4. TGA analysis

The thermal analyses of the prepared samples were carried out in nitrogen atmosphere (50 ml/min) in the temperature range of 25–700 °C with a heating rate of 10 °C/min using the TGA/DSC1, Mettler Toledo, Greifensee, Switzerland apparatus.

#### 2.4.5. POM analysis

POM analyses were performed with the use of a Lab40, Opta Tech, Warsaw, Poland microscope equipped with crossed polarizers and a MI20 Opta Tech, Warsaw, Poland camera combined with a LTS420, Linkam, Salfords, Great Britain heating stage. During the observations, a magnification of 500× was used. The heating rate was 5 °C/min.

#### 2.4.6. SEM analysis

Microscopic examinations were performed using a scanning electron microscope Phenom ProX, Thermo Scientific, Waltham, USA. The analysis was performed at a voltage of 15 kV using a BSD detector (Backscattered Electron Detector). Samples were fractured perpendicularly to the lines of the magnetic field applied during curing and their fracture surfaces were observed. The surface of the samples remained untreated.

#### 2.4.7. WAXS and SAXS analysis

X-ray scattering measurements were performed with a NanoStar-U diffractometer, Bruker, Billerica, USA with a 2D detector in transmission geometry. X-radiation of the wavelength  $\lambda = 1.54 \text{ \AA}$  were generated by a copper lamp, powered by 600  $\mu\text{A}$  at 50 kV. The instrument was equipped with two Göbel mirrors for monochromatization and parallelly aligning the beam of 500  $\mu\text{m}$  diameter. The measurements were carried out at room temperature. Scattering angles and intensity were determined with the use of Bruker AXS DIFFRAC > SAXS V.1.0 and Bruker AXS SAXS: Small Angle X-ray Scattering System V4.1.46 software.

#### 2.4.8. DS analysis

Dielectric spectroscopy tests were performed using a high-resolution Solartron 1260, Ametek, Berwyn, USA analyzer with a CDI Alpha attachment coupled with a Quatro Cryosystem, Novocontrol, Montabaur, Germany for measurements at low temperatures and a Linkam Salfords, Great Britain heating cell at high temperatures. The tested resin or ready-made polymer

samples were placed between parallel electrodes and tested in the frequency range of  $10^{-1}$ – $10^7$  Hz. All analyses were carried out at strictly controlled temperatures. The tests were carried out on solid cross-linked samples that were placed directly between metal electrodes. No additional conductive materials were used when preparing samples for measurements.

### 3. Results and discussion

#### 3.1. Confirmation of the structure of the synthesized resin

The NMR analysis was equipped to confirm the course of the chemical reaction performed and its result is visible in [Figure 2](#).

As presented in [Figure 2](#), all resonance signals were attributed to corresponding protons from the resin structure: isolated aliphatic chain (A-methyl, B-methylene group) in the region 0.75–1.75 ppm; methylene groups protons with signals shifted by ester formation (D, E) at 1.8 and 2.7 ppm; epoxy protons (C) at 2.9 ppm and aromatic ring protons (F–I) with different chemical shift caused by different magnetic neighbourhood. Moreover, the integrals presented in the [Figure 2](#) for the final product confirm the amount of hydrogen atoms in the molecules (integration of protons marked as 'I, H' is artificially elevated by the signal from the solvent –  $\text{CDCl}_3$ ). Spectra of intermediates and substrates allow to investigate the full course of the synthesis. Disappearance of the carboxylic protons from oleic acid (~11.5 ppm) and hydroxyl hydrogens (~10.7 ppm) from MEZO III on 4ANTVM spectrum proves that the esterification reaction has been completed. Subsequently, during oxidation of 4ANTVM, all of double C=C oleic acid bonds disappeared which is evidenced by the lack of signal at about 5.5 ppm in the 4ANTEM spectra as well as the presence of a signal at ~3.1 ppm, which should be attributed to protons from epoxy groups. Given all the analysed data, the synthesis can be described as successful.

#### 3.2. Thermal characteristics of curing substrates and LC nature of 4ANTEM resin

Investigated resin, like all novel compounds, needs thorough characterization in order to enable proper planning and performing the curing process. In the case of thermotropic liquid crystalline monomers, it is crucial to assess the range of mesophase stability,

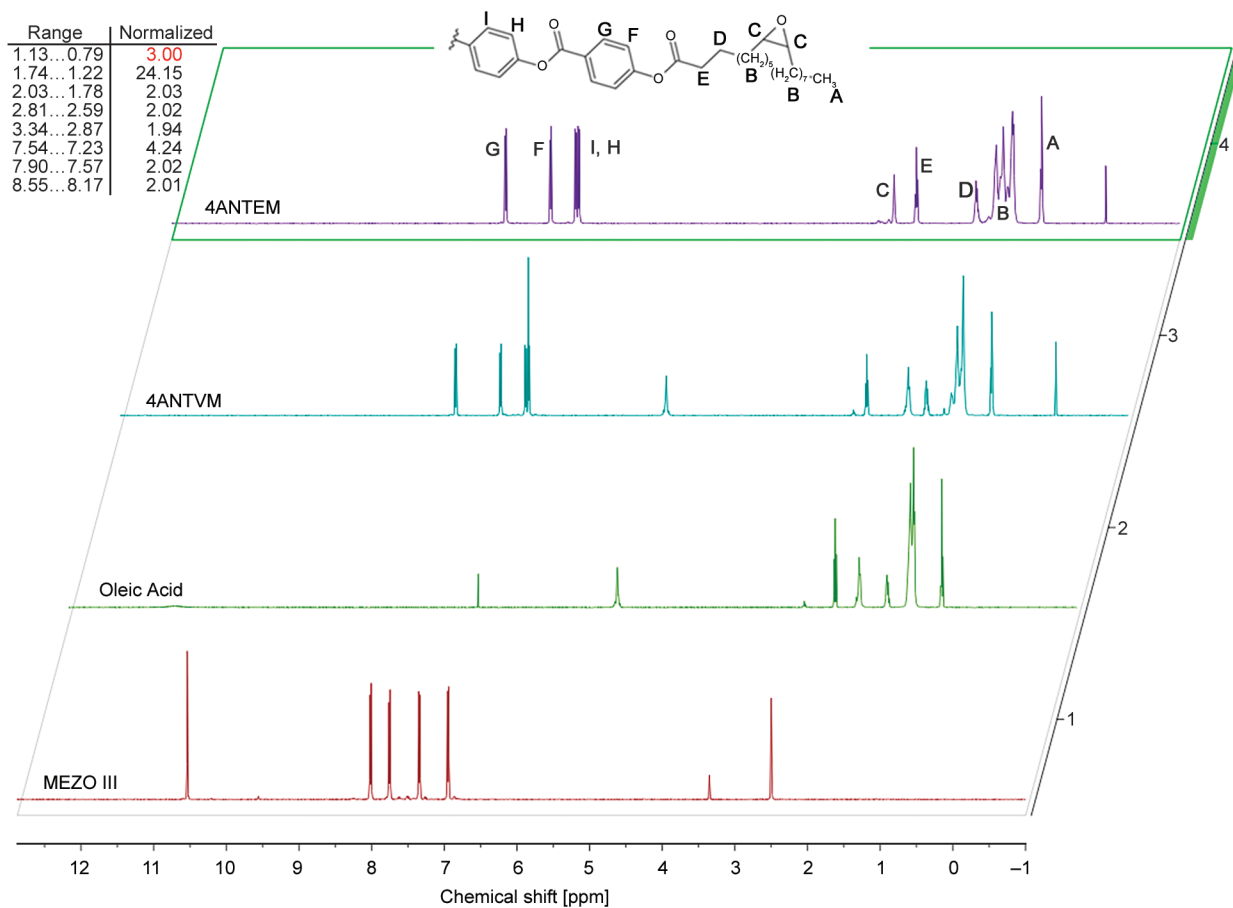


Figure 2. <sup>1</sup>H-NMR spectrum of synthesized 4ANTEM liquid crystalline epoxy resin.

because curing performed in that region of temperature allows to achieve molecularly ordered polymers.

A series of DSC analyses were performed to assess the thermal properties of substrates. The results are presented in Figure 3.

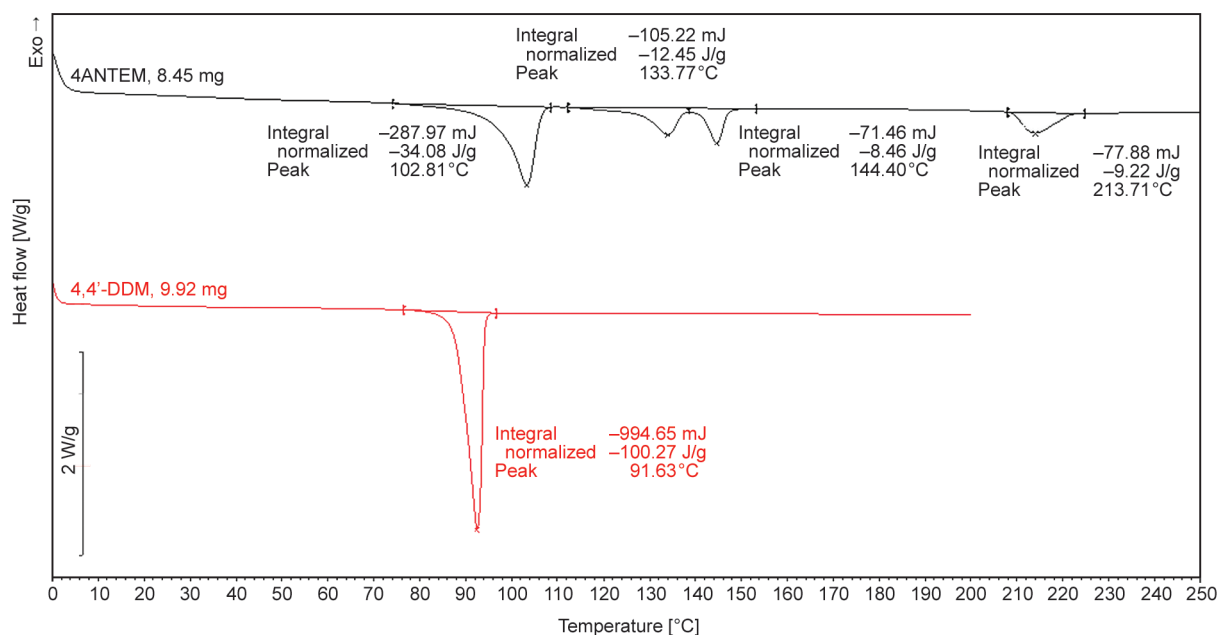
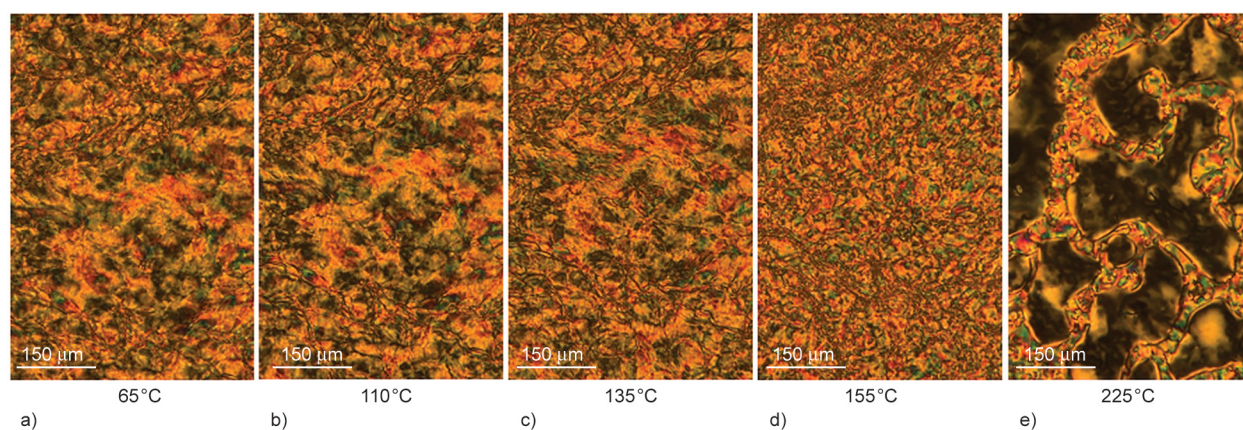


Figure 3. DSC thermal curves of pure 4ANTEM resin and 4,4'-DDM hardener.



**Figure 4.** POM microphotographs of 4ANTEM resin taken during heating with the following temperatures. a) Crystal 1 phase, b) crystal 2 phase, c) smectic phase, d) nematic phase, e) ongoing isotropisation.

The attached DSC thermograms show the melting process of a chosen hardener, 4,4'-DDM, at approximately 91.6 °C, which is consistent with data from the literature. A more complex phenomenon is visible for a synthesized resin, where four peaks are present on the thermogram recorded during heating. Previous research [24, 26] indicates that this should be a polymorphic transition (102.8 °C), then liquid crystal formation (133.8 °C), changes in LC phase (144.4 °C) and finally isotropisation at 213.7 °C. To confirm this for this novel, previously not synthesized compound, we performed POM (Figure 4).

Photographs presented confirm the liquid-crystalline nature of a compound and conclusions drawn from the DSC analysis. Every picture was taken after the phase transition recorded during the DSC analysis, and there is only little change between pictures Figure 4a and Figure 4b. This is typical for polymorphic transitions as they are difficult to detect with the use of the POM method. However, every next change is clear and produces typical textures for liquid crystals presenting decreasing level of order with a rise of the temperature (135 °C – smectic schlieren – layered structure with alignment along an axis; 155 °C – nematic marbled texture – aligned along an axis, but without distinct layers) [29]. At 225 °C the isotropisation process takes place, which is evidenced by black regions of view.

### 3.3. Analysis of a curing process

To analyze the curing process, we performed the DSC experiment for samples of mixture prepared to harden in Teflon molds. This was necessary to determine the glass transition temperature of the dynamically-hardened resin without the influence of the magnetic field for future reference. Moreover,

the shape of the thermal curve brings information about the intensity and temperature-range of the occurring reaction and allows the choice of possible conditions for isothermal curing assisted with the influence of the magnetic field. The thermogram presented in Figure 5 shows the chemical reaction that occurs between the epoxy and amine groups, as well as the transition characteristic for the substrates before the reaction.

The first two thermal effects can be attributed to the melting of an amine and the polymorphic change of 4ANTEM. Next, there is a deformed peak with maximum intensity at 136.4 °C, which shows a transition of an epoxy to a LC state. The deformation of this peak was studied by our team before [30], where we found that the curing reaction begins in the first moments of liquid crystal formation, and the overlapping exo-reaction and endo-transition give, as a result, a visible change in the thermal curve. Over 150 °C, of low intensity and with a wide temperature range, curing takes place, as evidenced by the detected heat of the reaction. Interestingly, this process intensifies at around 220 °C, which may indicate that isotropisation of a monomer lowers the viscosity of a mixture and facilitates curing. The investigated reaction is slow, so there was a need to find suitable isothermal conditions to cure larger samples fully. These investigations are presented in Figure 6.

To correlate with previous studies, we chose 3 h curing time. After this time, at selected temperatures, the second heating run was conducted to determine the extent of a cure. Residual peaks detected as a signal of unreacted resin meant that the temperature was too low. Finally, the 205 °C/3 h conditions were found to be optimal for the process of hardening. In our previous studies it was generally concluded that

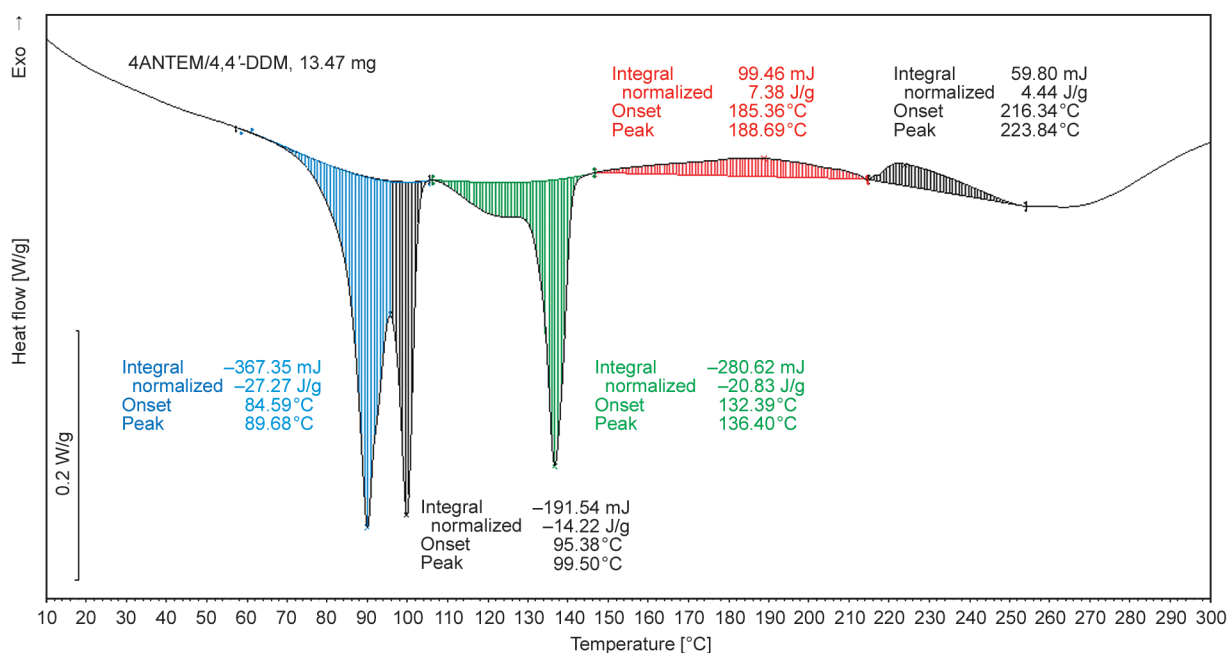


Figure 5. DSC thermogram of a curing of 4ANTEM/4,4'DDM system.

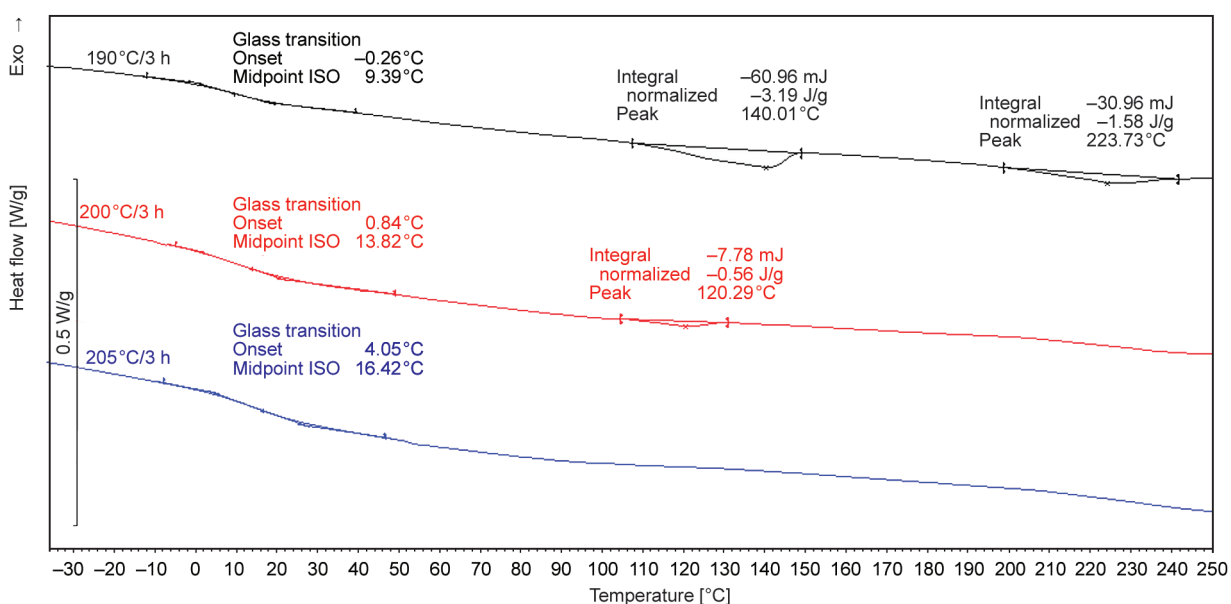


Figure 6. Second heating runs of isothermally cured 4ANTEM/4,4'-DDM samples.

the best conditions for inducing structural anisotropy is the lowest possible temperature, allowing to fully cure the mixture. DSC is a great tool to determine this temperature thanks to its sensitivity and very small samples, which gives economic advantages when compared to bigger samples prepared in molds. Simultaneously, the  $T_g$  of the synthesized thermoset was determined as 16.4°C (and, as expected, lower for non-fully cured samples). This is relatively low for a resin with a four-aromatic rigid core, and this can be explained by long, aliphatic spacers attached

to the mesogen, especially when the epoxy group is placed in the middle of the hydrocarbon chains, which may cause more steric hindrance. In effect, we get low crosslink density, which significantly lowers the glass transition temperature. This creates new possibilities, as it allows the polymer to work in the elastic state at room temperature.

### 3.4. Anisotropic polymer characterization

Molecularly ordered polymers were synthesized according to the procedure described in the materials

and methods section. A magnetic field induction of 1.2 T was used, as well as conditions without presence of the magnetic field, as a control sample.

### 3.4.1. Determination of $T_g$ and extent of cure

After the curing process had been completed, the samples were extracted from the molds and subjected to the DSC analysis. The results are presented in Figure 7.

Thermal curves in Figure 7 clearly show that the proposed time-temperature conditions are sufficient to fully harden the prepared samples. This is evidenced by the lack of thermal effects characteristic for substrates and for the exothermic curing process. The glass transition of the examined specimens is significantly different. For the sample cured without

an external magnetic field (black curve), the  $T_g$  is 16.9°C, which is consistent with previous DSC analyses (Figure 6). For the sample cured in the magnetic field with induction 1.2 T,  $T_g$  rises dramatically and reaches the value of 37.5°C. This is a visible sign of an important effect of the force field on the structure of the polymer. Glass transition temperature of cured epoxy resin is probably the most important thermal property alongside assessing the thermal stability of the obtained product, and both can be accurately determined with the use of DSC method.

Furthermore, to monitor the extent of the cure, FTIR analysis of the substrate and both synthesized samples was performed (Figure 8).

FTIR analysis provides additional proof that curing has been conducted successfully. This is clearly

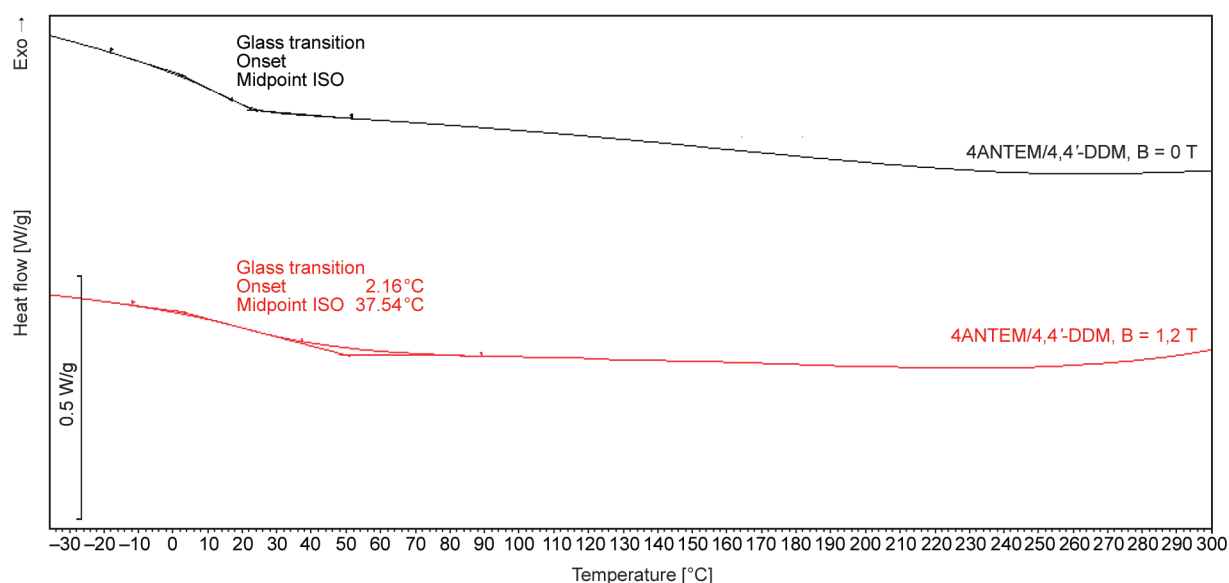


Figure 7. Thermograms of the thermosets cured in molds, with and without presence of the magnetic field.

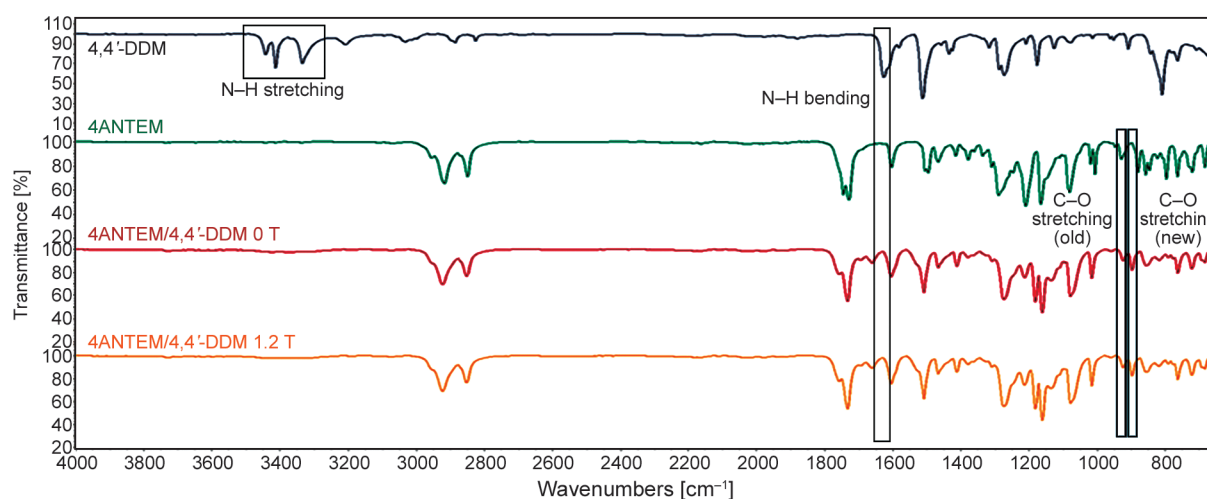


Figure 8. FTIR spectra of curing substrates and synthesized polymers.

evidenced by the disappearance or reduction of the intensity of the absorption bands considered diagnostic for the analysis of the described chemical reaction (marked with rectangles in the figure), especially vibrations of chemical bonds in the wavenumber range of  $3300\text{--}3500\text{ cm}^{-1}$  (N–H stretching) and at  $1630\text{ cm}^{-1}$  (N–H bending). There is also a visible drop in intensity for the  $920\text{ cm}^{-1}$  absorption band (coming from the stretching vibrations of the C–O bonds of the epoxy group), with the creation of a C–O stretching band at  $900\text{ cm}^{-1}$  as a sign of the formation of the new structural group resulted from breaking of oxirane ring [31]. It is worth noting that there are some residual bands, which show that conversion does not reach 100%, but epoxy networks, due to spatial restrictions, never allow all functional groups to react. This may influence the thermal stability of polymers and the difference between isotropic and anisotropic samples.

### 3.4.2. Thermal stability of synthesized samples

Due to the subtle rise of the DSC curve in the proximity of  $300\text{ }^{\circ}\text{C}$  (Figure 7) and the suspicion of starting thermal degradation in that region, the TGA analysis was conducted and the results are presented in Figure 9.

Based on the analysis performed, it can be concluded that the obtained polymers are characterized by good thermal resistance up to temperatures of approximately  $300\text{ }^{\circ}\text{C}$ , which, considering their intended use, is a very good result. The diagnostic parameter of 5%

mass loss is recorded at a temperature of  $351\text{ }^{\circ}\text{C}$  for the sample hardened without the presence of a magnetic field and  $343\text{ }^{\circ}\text{C}$  for the sample synthesized in the presence of this field. The thermal decomposition is characterized by an asymmetric peak, which indicates that this process may have a substage, and the maximum of its intensity falls at  $381\text{ }^{\circ}\text{C}$  (4ANTEM/4,4'-DDM 0T) and  $376\text{ }^{\circ}\text{C}$  (4ANTEM/4,4'-DDM 1.2 T). The mass loss in this stage of decomposition is 90.2 and 91.6%, respectively, and the remaining mass of the sample at  $700\text{ }^{\circ}\text{C}$  is 9.8 and 8.4%. Thus, the magnetic field slightly lowers the thermal stability of the polymer. However, this should not be a negative factor because of very small differences between samples and full stability up to over  $200\text{ }^{\circ}\text{C}$ , which is a rarely exceeded temperature for the operating range of polymeric materials. The differences between ordered and isotropic samples can be attributed to different morphology of networks, which causes different distributions of free, easy-to-detach functional groups with temperature. Alignment with the magnetic field forces the molecules to remain in a specific position, so it can restrict some access to the reactive centers during curing, leaving the resulting polymer slightly more susceptible to thermal degradation. It seems that enhancement of investigated properties by inducing molecular order in this particular case cannot be achieved because of additional and artificially generated steric obstacles, but as it was mentioned before, this minor negative influence should not be a decisive factor also because of its

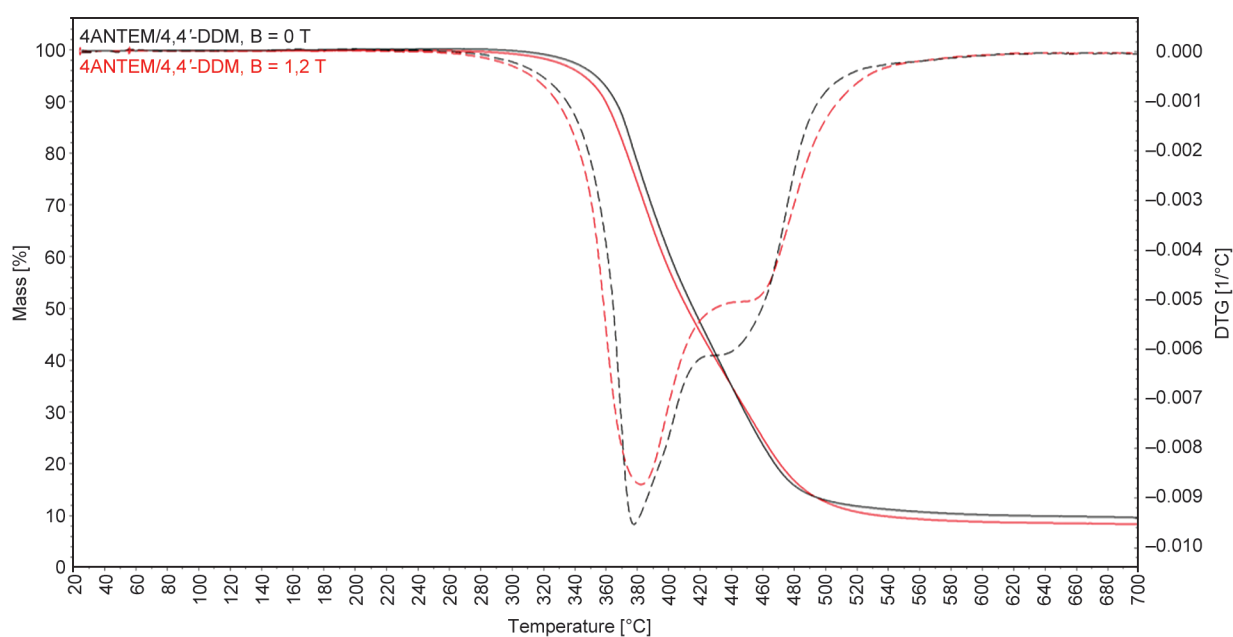


Figure 9. TGA curves for synthesized 4ANTEM/4,4'-DDM 0 T and 4ANTEM/4,4'-DDM 1.2 T samples.

very limited presence. When the curing is performed without magnetic field, and the reaction undergoes in a more chaotic manner without obstacles coming from orientational order, there may be a possibility of easier contact of amine and epoxy groups attached to monomers elastic chains with great mobility within the sample volume.

### 3.4.3. Morphology of polymers – SEM

To assess the morphological characteristics of the obtained polymers, we used SEM analysis. The microphotographs are presented in Figure 10.

SEM analysis gives solid proof of the influence of the magnetic field on the structure of the obtained thermosets. Left and right pictures are the magnifications of the middle photographs. Both samples present morphology characteristics for the liquid crystal domain [32], so it can be stated that the magnetic field does not induce this phase, but it is clear that it induces molecular order. There are parts of parallel layers of domains visible in the photographs of thermosets synthesized in the magnetic field (red circle),

which is characteristic of the smectic liquid crystal [33]. There are also typical for liquid crystalline polymers abruptsions of fracture propagation (blue ellipses) [32], so it can be firmly stated that synthesized samples are of liquid crystalline nature. To fully assess the molecular order of achieved polymers, the WAXS analysis was used.

### 3.4.4. Morphology of polymers – WAXS and SAXS analysis

To prove findings concerning the molecular order of the presented thermoset detected by SEM observations and noted differences in properties, the WAXS scattering data was collected and presented in Figure 11.

The analysis of presented diffractograms shows that the structure of the synthesized polymers is somewhat similar, but some level of molecular order was achieved. This is less noticeable with only visual interpretation of 2D pattern where only subtle nonuniformity of diffraction intensity can be noticed. Additionally, the integration of intensity within the

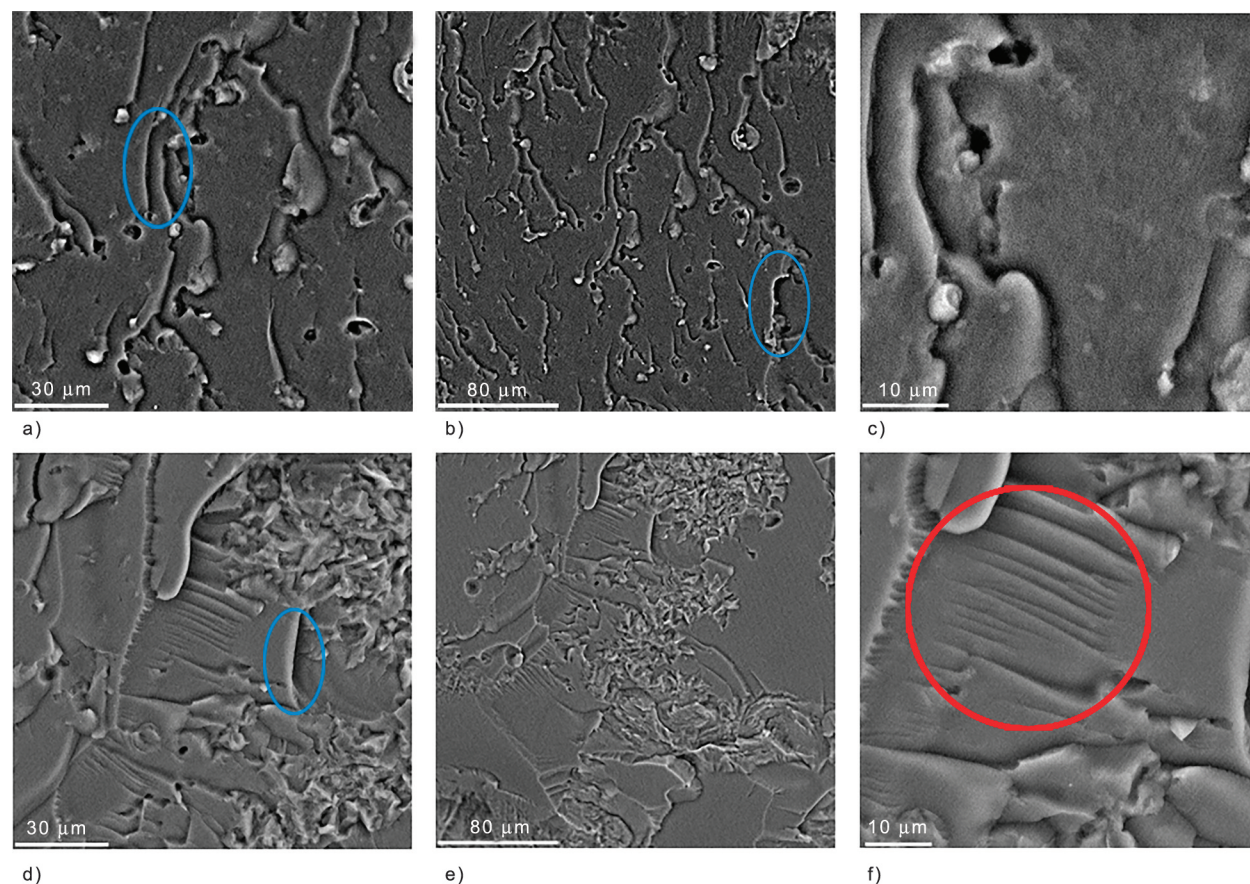


**Figure 10.** SEM microphotographs of fracture surfaces of 4ANTEM/4,4'-DDM 0 T. a) 4ANTEM/4,4'-DDM 0 T, magnification 2000×. b) 4ANTEM/4,4'-DDM 0 T, magnification 1000×, c) 4ANTEM/4,4'-DDM 0 T, magnification 5600×, d) 4ANTEM/4,4'-DDM 1.2 T, magnification 2000×, e) 4ANTEM/4,4'-DDM 1.2 T, magnification 1000×, f) 4ANTEM/4,4'-DDM 1.2 T, magnification 4500×.

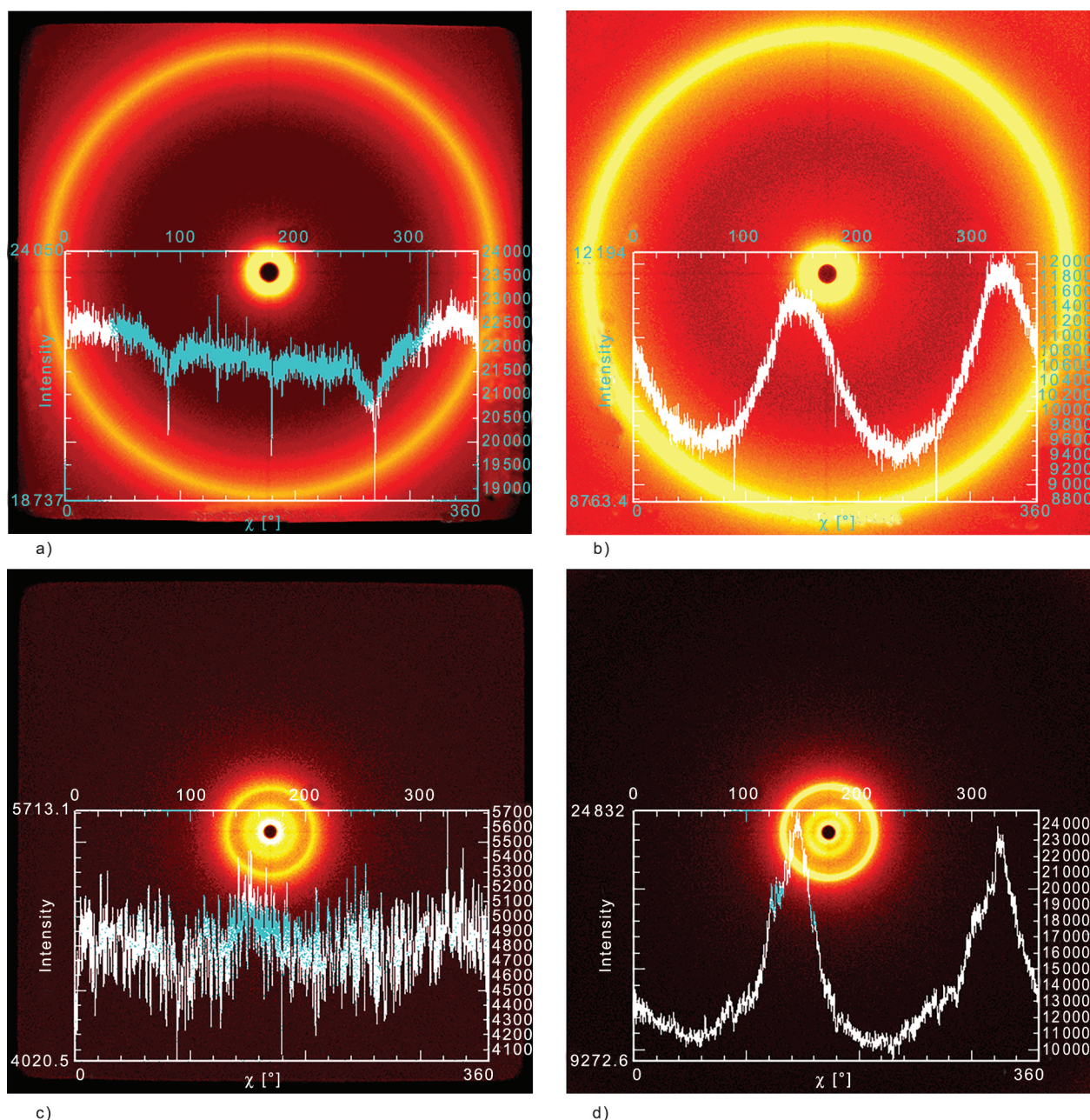


**Figure 11.** WAXS and SAXS scattering patterns of 4ANTEM/4,4'-DDM 0 T (a, c) and 4ANTEM/4,4'-DDM 1.2 T (b, d) samples.

17.2–21.5°  $\theta$  angle range was performed and presented on the intensity as the function of  $\chi$  angle plot. This shows that in the case of the sample prepared without magnetic field (Figure 11a) the scattering intensity is almost uniform within 360°  $\chi$  range. There are abrupt, local changes in the presented function, but they are caused by a beamstop holder, not by a sample. This holder can be seen on both 2D patterns as crosshair-like thin, darker lines. Polymer cured in the presence of magnetic field (Figure 11b) presents different characteristics. Some level of ordering is proved by the sinusoidal form of the plotted function with the intensity ranging from 9200 to

12 000 counts, which gives around 30% difference. The ordering is substantial enough to eliminate the beamstop effect on the results.

Interpretation of the SAXS results, contrary to WAXS, allows even to visually detect deformations of the diffraction rings in the patterns caused by molecular alignment in the case of polymer synthesized with the presence of magnetic field (Figure 11d). Analysis of  $\theta$  angle range below 2°, where scattering intensity takes values from 10 000 to 24 000 (140% difference), definitively proves that the obtained sample has an anisotropic structure. The sample prepared without magnetic field (Figure 11c) presents no

significant signs of molecular order, and scattering intensity is somewhat uniform with visible beamstop influence. The differences in the level of ordering between SAXS and WAXS studies can be explained by comparing these two techniques [34–36]. SAXS, as it describes smaller  $\theta$  angles, can evaluate a bigger part of LC-network structure, which is determined by oriented mesogens. WAXS, describing smaller parts and dimensions of the structure, takes into account also individual loose aliphatic chains not susceptible to the magnetic field. This is important in the case of proposed polymers because network nodes are in the middle of aliphatic chains of the monomer, which gives those spacers more mobility, which can lower the determined level of anisotropy. During X-ray analysis, the scattering intensity as a function of the magnitude of the scattering vector plot was also prepared for both samples and presented in Figure 12.

The course of the function clearly differs for both samples, which proves that magnetic field changes the scattering patterns, and this has to be caused by induced molecular orientation because the composition of both samples is the same. The first difference is noticeable in the  $q$  values of 0.05–0.20  $\text{\AA}^{-1}$ , which corresponds to structural components of the polymer with the size of about 35–60  $\text{\AA}$ , which should be attributed to the possible length of the 4ANTEM molecule with regard to the fact that aliphatic chains remain loosely attached. Moreover, the sample cured in the magnetic field, contrary to the second polymer, presents an almost uniform peak, with only one clear maximum, so it can be concluded that ordering has been achieved. Another difference is detected at  $q$  in the range of 1.25–1.55. The isotropic sample presents a local scattering maximum at  $q = 1.30 \text{\AA}^{-1}$  (part of the structure with  $\sim 4,85 \text{\AA}$  width) and an anisotropic one at  $q = 1.51 \text{\AA}^{-1}$  ( $\sim 4,15 \text{\AA}$  width).

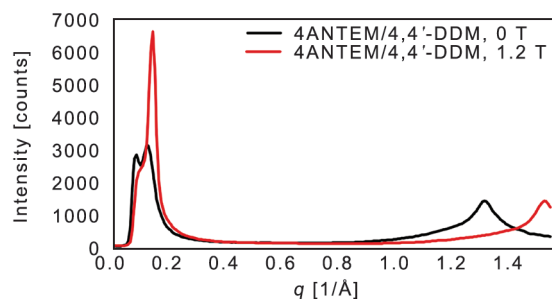


**Figure 12.** Scattering intensity plot as a function of magnitude of scattering vector for investigated polymers.

These kinds of dimensions are characteristic of lateral distances of aromatic cores, and a slightly smaller value for the sample cured with magnetic field means that molecules are more packed, which is explained by molecular orientation [26].

It has to be noted, however, that the achieved level of structural anisotropy is smaller than can be achieved in the case of other LC-epoxies prepared also by our team [24, 26], but substantial enough to facilitate important shift in properties, which is always the most important goal.

### 3.4.5. Dielectric properties

Dielectric characterization was conducted to assess the possible use of prepared polymers in low-weight electronic devices. As the polymers are designed to be highly elastic due to long dangling aliphatic chains and low crosslink density (low epoxy equivalent as a result of the structure of the monomer), we aimed to synthesize durable, elastic polymer with an electrically-related potential of liquid crystals. In our recent paper [28], for similar resin, we noticed additional, when compared to earlier studies, dielectric relaxation process, so it was also necessary to confirm its presence in the investigated four-aromatic resin as it is material not described before. The abrupt changes of conductivity for those materials are correlated with the vitrification process, so dielectric studies were also used to confirm conclusions drawn from the DSC data.

The results for hardened materials were obtained during cooling from high temperatures to  $-50 \text{ }^\circ\text{C}$ . The obtained values of the real and imaginary components of electrical permeability are presented in Figure 13.

Both the values of electrical permeability and conductivity change significantly with the change in temperature. Noteworthy, the rapid increase in conductivity at temperatures above  $25 \text{ }^\circ\text{C}$  was obtained for both samples, which can be seen in detail in Table 1. This increase is detected in slightly lower temperatures for samples cured without magnetic field as this is probably related to less-constraint mobility of LC-units in not ordered structure. It is also possible to notice a certain shift in the  $\alpha$ -process (related to the glass transition temperature) for the sample crosslinked in a magnetic field compared to samples crosslinked without this factor. Additionally, at low temperatures, two processes are visible that can be interpreted as relaxations of local dipole groups:

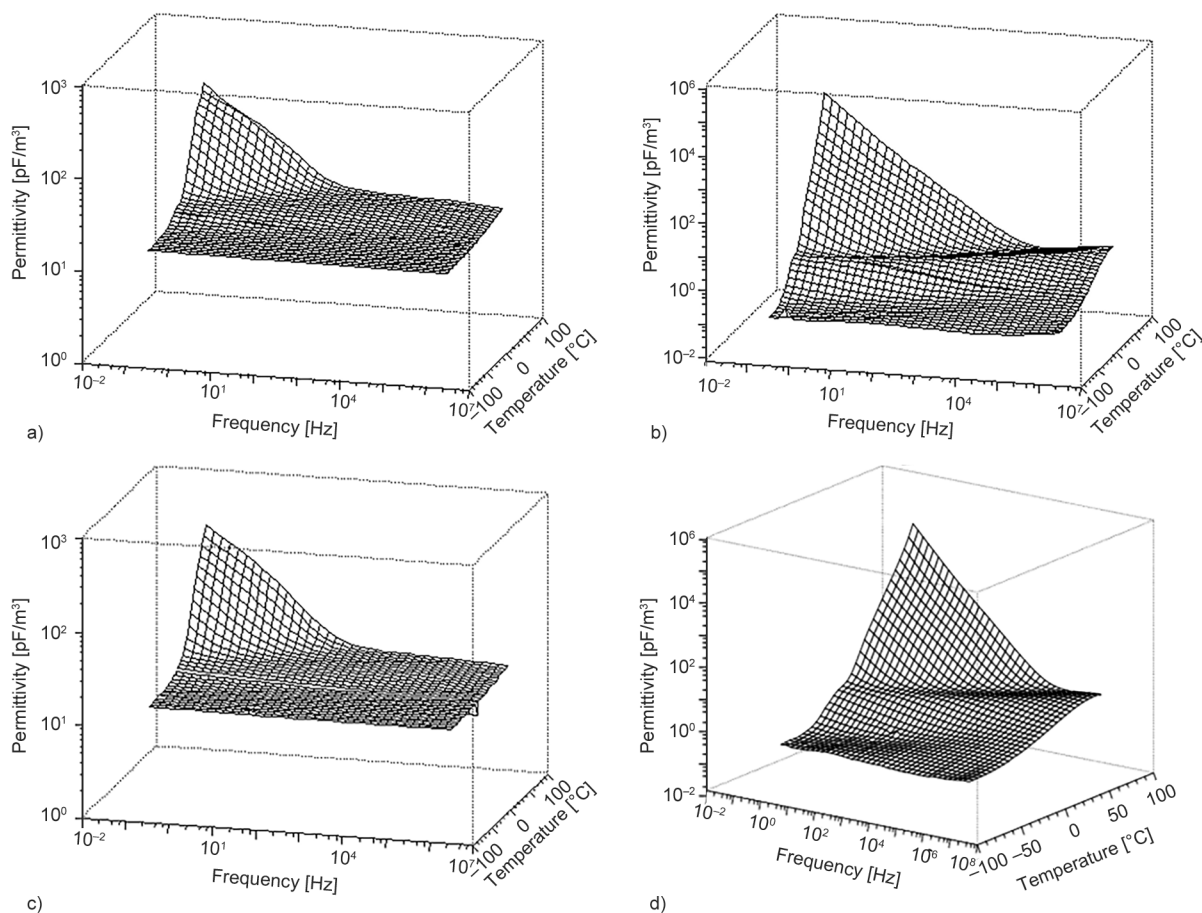


**Figure 13.** Dielectric response (electrical permittivity) for the hardened material in a wide range of frequencies and temperatures: a) real part – 4ANTEM/4,4'-DDM 0 T, b) imaginary part – 4ANTEM/4,4'-DDM 0 T, c) real part – 4ANTEM/4,4'-DDM 1.2 T, d) imaginary part – 4ANTEM/4,4'-DDM 1.2 T.

one related to certain mobility of the mesogen, the other to the mobility of carbon chains. For a polymer hardened in a magnetic field, these phenomena are less visible, and some minor shifts in relaxations are also visible. As the described relaxation processes are related to the motion of polymer chains or their parts, the presented results are additional proof that molecular arrangement has been achieved with the utilization of the magnetic field. Anisotropic polymer undergoes vitrification at higher temperatures, and parts of their structure are also more constrained, which is evidenced by less visible processes than in

the case of isotropic samples. The described results also confirm our previous studies [28] due to visible relaxation in the lowest temperature region of the analysis. This was not detected for resins with terminal epoxy groups, because it is correlated with flexibility of loose carbon chains and greater elasticity of the polymer caused also by lower crosslink density. The change in structure, therefore, causes modifications in the dielectric properties of the sample – molecular orientations bring constraint to chain mobility, which results in a shift in rise of electrical conductivity to higher temperature (this is linked to higher

**Table 1.** Selected values of electrical permittivity (determined for the frequency  $f = 1$  kHz) and direct current conductivity of the 4ANTEM/4,4'-DDM 0 T and 4ANTEM/4,4'-DDM 1.2 T samples.

Temperature [°C]	4ANTEM/4,4'-DDM 0 T		4ANTEM/4,4'-DDM 1.2 T	
	Electric permeability [pF/m]	Electric conductivity [S/m]	Electric permeability [pF/m]	Electric conductivity [S/m]
-40	97.394	$5 \cdot 10^{-16}$	88.540	$1 \cdot 10^{-16}$
5	106.248	$5 \cdot 10^{-15}$	97.394	$1 \cdot 10^{-15}$
25	115.102	$5 \cdot 10^{-14}$	106.248	$1 \cdot 10^{-14}$
50	132.810	$1 \cdot 10^{-12}$	123.956	$1 \cdot 10^{-12}$
100	150.518	$1 \cdot 10^{-9}$	141.664	$1 \cdot 10^{-9}$

$T_g$ ), but simultaneously incorporation of oleic acid in the structure of the resin makes it more susceptible to relaxation facilitated by dangling hydrocarbon chains. Moreover, a bigger mesogenic core, consisting of four aromatic rings instead of three, shifts the processes to higher temperatures by stiffening the structure.

#### 4. Conclusions

A new kind of liquid crystalline epoxy resin with four-aromatic core, not described previously in the literature, characterized by epoxy groups in the middle of the aliphatic spacer chains, was successfully synthesized and cured with an aromatic amine – 4,4'-diaminodiphenylmethane. The curing process was studied, and samples of the polymer were prepared under optimal conditions with and without the presence of the strong (1.2 T) external magnetic field.

It has been confirmed that the magnetic field influences all investigated properties of the samples by lifting  $T_g$  for about 20 °C, slightly lowering thermal stability, influencing polymer morphology by inducing molecular order and causing changes in electrical properties. However, it seems that it does not influence significantly the extent of the cure and, thanks to that fact, it is convenient to determine optimal curing conditions for all methodologies.

A structurally ordered polymer, with  $T_g$  of 37.5 °C, thermally stable up to over 300 °C and with increased conductivity (compared to glassy product) just above room temperature has been possible to achieve. The change in properties with temperature is especially important because it makes this material an innovative candidate for tailored, smart material working in proximity of ambient temperature. With just a slight heating caused by a pulse from a laser, heat dissipated from electrical resistance or a simple temperature rise of the environment, it is possible to change its properties and reverse this process later by cooling. This smart property creates new application possibilities, especially in avionics, where lightweight and elastic yet durable, crosslinked polymer materials with low  $T_g$  should be preferred over dense and heavy metals. Moreover, with a magnetic field it is possible to change the temperature that changes the properties of synthesized polymer.

#### Acknowledgements

The research leading to these results has received funding from the commissioned task entitled 'VIA CARPATIA Universities of Technology Network named after the President of the Republic of Poland Lech Kaczyński' contract no. MEiN/2022/DPI/2578, action entitled 'In the neighborhood – inter-university research internships and study visits'.

#### References

- [1] Mohan P.: A critical review: The modification, properties, and applications of epoxy resins. *Polymer-Plastics Technology and Engineering*, **52**, 107–125 (2013).  
<https://doi.org/10.1080/03602559.2012.727057>
- [2] Srivastava A. K., Mohan P.: Synthesis, reactions, and properties of modified epoxy resins. *Journal of Macromolecular Science Part C: Polymer Reviews*, **37**, 687–716 (1997).  
<https://doi.org/10.1080/15321799708009653>
- [3] Liu Y. L., Chiu Y. C., Wu C. S.: Preparation of silicon-/phosphorous-containing epoxy resins from the fusion process to bring a synergistic effect on improving the resins' thermal stability and flame retardancy. *Journal of Applied Polymer Science*, **87**, 404–411 (2003).  
<https://doi.org/10.1002/app.11383>
- [4] Wang J-S., Wang D-Y., Liu Y., Ge X-G., Wang Y-Z.: Polyamide-enhanced flame retardancy of ammonium polyphosphate on epoxy resin. *Journal of Applied Polymer Science*, **108**, 2644–2653 (2008).  
<https://doi.org/10.1002/app.27522>
- [5] Du Y., Zhao G., Shi G., Wang Y., Li W., Ren S.: Effect of crosslink structure on mechanical properties, thermal stability and flame retardancy of natural flavonoid based epoxy resins. *European Polymer Journal*, **162**, 110898 (2022).  
<https://doi.org/10.1016/j.eurpolymj.2021.110898>
- [6] Unnikrishnan K. P., Thachil E. T.: The modification of commercial epoxy resin using cardanol – Formaldehyde copolymers. *International Journal of Polymeric Materials*, **55**, 323–338 (2006).  
<https://doi.org/10.1080/009140390945178>
- [7] Li Y., Ambrogi V., Cerruti P., Goswami M., Yang Z., Kessler M. R., Rios O.: Functional liquid crystalline epoxy networks and composites: From materials design to applications. *International Materials Reviews*, **67**, 201–229 (2022).  
<https://doi.org/10.1080/09506608.2021.1937811>
- [8] Kisiel M., Mossety-Leszczak B.: Development in liquid crystalline epoxy resins and composites – A review. *European Polymer Journal*, **124**, 109507 (2020).  
<https://doi.org/10.1016/j.eurpolymj.2020.109507>

- [9] Mossety-Leszczak B., Kisiel M.: Liquid crystalline polymers. in ‘Thermal analysis of polymeric materials’ (eds.: Pieliowski K., Pieliowska K.) Wiley, Weinheim, Vol. 1, 381–408 (2022).  
<https://doi.org/10.1002/9783527828692.ch10>
- [10] Kim Y., Kim H., Choi J.: Mechanical origin of shape memory performance for crosslinked epoxy networks. *European Polymer Journal*, **194**, 112162 (2023).  
<https://doi.org/10.1016/j.eurpolymj.2023.112162>
- [11] Amendola E., Carfagna C., Giamberini M., Komitov L.: Anisotropic liquid crystalline epoxy thermoset. *Liquid Crystals*, **21**, 317–325 (1996).  
<https://doi.org/10.1080/02678299608032840>
- [12] Harada M., Ochi M., Tobita M., Kimura T., Ishigaki T., Shimoyama N., Aoki H.: Thermal-conductivity properties of liquid-crystalline epoxy resin cured under a magnetic field. *Journal of Polymer Science Part B: Polymer Physics*, **41**, 1739–1743 (2003).  
<https://doi.org/10.1002/polb.10531>
- [13] Wang T., Wang J., Liao G., Wang W., Qiu Y., Yin G., Liao Y., Xie X.: Flexible films of main-chain luminescent liquid crystalline polymers containing renewable biobased bifuran moieties. *European Polymer Journal*, **199**, 112448 (2023).  
<https://doi.org/10.1016/j.eurpolymj.2023.112448>
- [14] Hussain F., Fayzan Shakir H. M., Ali A., Rehan Z. A., Zubair Z.: Development and characterization of cyclic compound-based biaxially stretched smart polymeric film for futuristic flexible electronic devices. *European Polymer Journal*, **172**, 111243 (2022).  
<https://doi.org/10.1016/j.eurpolymj.2022.111243>
- [15] Saraswat A., Kumar S.: Cutting-edge applications of polyaniline composites towards futuristic energy supply devices. *European Polymer Journal*, **200**, 112501 (2023).  
<https://doi.org/10.1016/j.eurpolymj.2023.112501>
- [16] Yang H., Yuan G., Jiao E., Wang K., Diao W. J., Li Z., Wu K., Shi J.: Low dielectric constant and high thermal stability of liquid crystal epoxy polymers based on functionalized poly(phenylene oxide). *European Polymer Journal*, **198**, 112378 (2023).  
<https://doi.org/10.1016/j.eurpolymj.2023.112378>
- [17] Wang S., Ma S., Li N., Jie S., Luo Y., Gao X.: Branched thermotropic liquid crystal polymer with favourable processability and dielectric properties. *European Polymer Journal*, **196**, 112302 (2023).  
<https://doi.org/10.1016/j.eurpolymj.2023.112302>
- [18] Kim H. C., Mun S., Ko H-U., Zhai L., Kafy A., Kim J.: Renewable smart materials. *Smart Materials and Structures*, **25**, 073001 (2016).  
<https://doi.org/10.1088/0964-1726/25/7/073001>
- [19] Kakiuchida H., Ogiwara A.: Reverse-mode thermoresponsive light attenuators produced by optical anisotropic composites of nematic liquid crystals and reactive mesogens. *Optical Materials*, **78**, 273–278 (2018).  
<https://doi.org/10.1016/j.optmat.2018.01.046>
- [20] Guo H., Li Y., Zheng J., Gan J., Liang L., Wu K., Lu M.: High thermo-responsive shape memory epoxies based on substituted biphenyl mesogenic with good water resistance. *RSC Advances*, **5**, 67247–67257 (2015).  
<https://doi.org/10.1039/c5ra10957d>
- [21] Guo H., Li Y., Zheng J., Gan J., Liang L., Wu K., Lu M.: Reinforcement in the mechanical properties of shape memory liquid crystalline epoxy composites. *Journal of Applied Polymer Science*, **132**, 42616 (2015).  
<https://doi.org/10.1002/app.42616>
- [22] Chow W. S., Mohd Ishak Z. A.: Smart polymer nanocomposites: A review. *Express Polymer Letters*, **14**, 416–435 (2020).  
<https://doi.org/10.3144/expresspolymlett.2020.35>
- [23] Vallejo-García J. L., Arnaiz A., Busto M. D., García J. M., Vallejos S.: Film-shaped reusable smart polymer to produce lactose-free milk by simple immersion. *European Polymer Journal*, **200**, 112495 (2023).  
<https://doi.org/10.1016/j.eurpolymj.2023.112495>
- [24] Kisiel M., Mossety-Leszczak B., Strachota B., Strachota A.: Achieving structural anisotropy of liquid crystalline epoxy by manipulation with crosslinking parameters. *Express Polymer Letters*, **15**, 274–287 (2021).  
<https://doi.org/10.3144/expresspolymlett.2021.24>
- [25] Mossety-Leszczak B., Pilch-Pitera B., Karaś J., Kisiel M., Zając W., Włodarska M.: The application of liquid crystalline epoxy resin for forming hybrid powder coatings. *Progress in Organic Coatings*, **168**, 106873 (2022).  
<https://doi.org/10.1016/j.porgcoat.2022.106873>
- [26] Mossety-Leszczak B., Kisiel M., Szałański P., Włodarska M., Szeluga U., Pusz S.: The influence of a magnetic field on the morphology and thermomechanical properties of a liquid crystalline epoxy carbon composite. *Polymer Composites*, **39**, 2573–2583 (2018).  
<https://doi.org/10.1002/pc.24848>
- [27] Włodarska M., Mossety-Leszczak B., Bąk G. W., Kisiel M., Dłużniewski M., Okrasa L.: Epoxy matrix with triaromatic mesogenic unit in dielectric spectroscopy observation. *Spectrochimica Acta Part A: Molecular and Biomolecular Spectroscopy*, **194**, 102–110 (2018).  
<https://doi.org/10.1016/j.saa.2018.01.001>
- [28] Włodarska M., Mossety-Leszczak B., Kisiel M., Zając W., Okrasa L.: Changes in molecular relaxations and network properties of a triaromatic liquid crystal epoxy resin with nonterminal functional groups. *Journal of Polymer Science*, **61**, 3244–3255 (2023).  
<https://doi.org/10.1002/pol.20230351>
- [29] Dierking I.: Textures of liquid crystals. Wiley, Weinheim (2003).
- [30] Mossety-Leszczak B., Kisiel M., Lechowicz J. B., Buszta N., Ostatek R., Włodarska M.: Analysis of curing reaction of liquid-crystalline epoxy compositions by using temperature-modulated DSC TOPEM®. *Journal of Thermal Analysis and Calorimetry*, **138**, 2435–2444 (2019).  
<https://doi.org/10.1007/s10973-019-08193-w>

- [31] González M. G., Cabanelas J. C., Baselga J.: Applications of FTIR on epoxy resins – Identification, monitoring the curing process, phase separation and water uptake. in ‘Infrared spectroscopy – Materials science, engineering and technology’ (ed.: Theophanides T.) In-echOpen, London, 261–281 (2012).  
<https://doi.org/10.5772/36323>
- [32] Kessler M. R., Li Y., Zhang Y., Rios O.: Advances in multifunctional liquid crystalline networks. Video Proceedings of Advanced Materials, **2**, 2021–0192 (2021).  
<https://doi.org/10.5185/vpoam.2021.0192>
- [33] Vertongen G., de Jeu W. H.: Thermotropic liquid crystals, fundamentals. Springer, New York (1988).
- [34] Cullity B. D., Cohen M.: Elements of X-ray diffraction. Addison-Wesley, Boston (1978).
- [35] Yang R.: Analytical methods for polymer characterization. CRC Press, Boca Raton (2018).
- [36] Bragg W. H., Bragg W. L.: The reflection of X-rays by crystals. Proceedings of the Royal Society A: Mathematical, Physical and Engineering Sciences, **88**, 428–438 (1913).  
<https://doi.org/10.1098/rspa.1913.0040>